Supplementary Information

Vacancy order beyond complete local coordination in perovskites

Jiasheng Yang
Sino-European School of Technology, Shanghai University, Shanghai 200444, China

Contents

Supplementary Note: Parent adjacency, Fourier conventions and real compatibility
Supplementary Note: Complete finite-support kernel
Supplementary Note: Periodic decomposition and dimensions
Supplementary Note: Binary constructions and complete restricted classifications
Supplementary Note: Capacity rigidity, dual criterion and nonlocal saturation
Supplementary Note: Hidden-coordinate geometry, counting and structural distance
Supplementary Note: Domain restriction and defect moments
Supplementary Note: Complete single-layer channel and exact switching extremum
Supplementary Note: Pbam coordinate mappings and registry constructions
Supplementary Note: Homologous vacancy planes and intergrowth
Supplementary Note: Pnma $CaMnO_{2.75}$ descriptor example
Supplementary Note: Reciprocal contrast, public ideal structures and homometry
Supplementary Note: Verification, data provenance and inheritance
Supplementary Note: Experimental minimal rigid topology in $CaMnO_{2.5}$
Supplementary Tables S1–S6
Supplementary References
Supplementary Figures and legends S1–S5

Supplementary Note: Parent adjacency, Fourier conventions and real compatibility

Occupation variables and neighbour shells

Let e_x, e_y, e_z be the unit basis of the integer parent lattice. B sites are labelled by $n \in \mathbb{Z}^3$, A sites have positions $n + a$ with $a = (1/2, 1/2, 1/2)$, and an oxygen site of type j has position $n + e_j/2$. We retain this inherited incidence relation when a refined crystal is mapped to the parent. Thus the word coordination in the calculation refers to occupation of these neighbours.

The variable $x_j(n) = 1$ denotes a vacant oxygen site and $x_j(n) = 0$ an occupied site. For linear calculations it may also be real. An oxygen vacancy at the j edge anchored at n contributes one missing oxygen to B at n and $n + e_j$, and to A with integer labels $n - pe_k - qe_l$, $p, q \in \{0, 1\}$, $\{j, k, l\} = \{x, y, z\}$. Therefore

$$(C_B x)(n) = \sum_j [x_j(n) + x_j(n - e_j)], \qquad (C_A x)(n) = \sum_j \sum_{p,q=0}^{1} x_j(n + pe_k + qe_l). \tag{S1}$$

Write $C = (C_B, C_A)^T$ and $f = (f_B, f_A)^T$. The parent coordination numbers are $6 - f_B$ and $12 - f_A$. For finite changes, or for one whole periodic unit,

$$\sum_n f_B(n) = 2 \sum_{n,j} x_j(n), \qquad \sum_n f_A(n) = 4 \sum_{n,j} x_j(n). \tag{S2}$$

For binary $f_B = 1$, vacancy edges form a perfect matching of the B graph. The additional equation $f_A = 2$ requires exactly two vacancy edges on the twelve-edge parent cube surrounding each A site. These are constraints on the same edge set. They are not two independently chosen matchings.

The crystallographic literature establishes ordered oxygen-deficient perovskite structures [1,2,3,4,5,6]. Group-theoretical enumeration classifies anion-order symmetries [7]. Our fixed object is the simultaneous map in (S1); neither a coordination histogram nor a space-group label replaces it.

Physical-basis Fourier convention

For finite-support fields define

$$X_j(k) = \sum_n x_j(n) e^{-ik\cdot(n+e_j/2)}, \quad F_B(k) = \sum_n f_B(n) e^{-ik\cdot n}, \quad F_A(k) = \sum_n f_A(n) e^{-ik\cdot(n+a)}. \tag{S3}$$

For a periodic unit with N parent cells, insert the common factor $N^{-1/2}$ when a unitary transform is needed for norms. Equations involving amplitudes use either normalization consistently on both sides.

The two B endpoints of a j edge give $2\cos(k_j/2)$. The four A neighbours give $4\cos(k_k/2)\cos(k_l/2)$. Hence

$$F(k) = C(k)X(k), \qquad C(k) = \begin{pmatrix} 2c_x & 2c_y & 2c_z \\ 4c_yc_z & 4c_xc_z & 4c_xc_y \end{pmatrix}, \quad c_j = \cos(k_j/2). \tag{S4}$$

This real symbol is a physical-basis representation. On crossing a parent reciprocal-lattice vector, the oxygen basis amplitudes acquire their corresponding phase factors. A plotted Brillouin-zone boundary therefore has identified faces with a basis gauge. In calculations one either keeps signed wavevectors and conjugate pairs, or carries those gauge factors when choosing a single representative. The squared norm of a vector amplitude is invariant under this rephasing.

Complete rank classification

The three 2×2 minors, apart from orientation signs, are

$$8c_z(c_x^2 - c_y^2), \quad 8c_x(c_y^2 - c_z^2), \quad 8c_y(c_z^2 - c_x^2). \tag{S5}$$

Choose $k_j \in [-\pi, \pi]$, so $c_j \geq 0$. If all c_j are nonzero, all minors vanish precisely when $c_x = c_y = c_z$. This gives the four signed body diagonals. If precisely one cosine is zero, a minor containing the other nonzero factors is nonzero and the rank remains two. If precisely two cosines are zero, only the B row has one nonzero entry, so the rank is one: these are the three zone-edge lines. If all three vanish, C=0 at $R = (\pi, \pi, \pi)$. There are no remaining cases. We call their union Σ.

On a diagonal, $C_A = 2\cos(t/2)C_B$. On an edge $C_A = 0$. At R both rows vanish. Thus a real periodic target has a real occupation solution if and only if its Fourier components satisfy

$$F_A = 2\cos(t/2)F_B \text{ on diagonals}, \quad F_A = 0 \text{ on edges}, \quad F_A = F_B = 0 \text{ at R}. \tag{S6}$$

No additional row condition occurs at rank-two points. Sufficiency follows by solving each finite-dimensional image problem, for example with a Moore–Penrose inverse, then imposing the compatible conjugacy of X

at paired characters. This constructs a real field. Equations (S6) describe real-linear compatibility; the intersection of that affine solution space with [0,1] or {0,1} is a further problem.

A separately feasible but jointly infeasible target

On an L=4 cubic torus put $s = n_x+n_y+n_z$ mod 4. Let $f_B = 1$ and prescribe $f_A(s) = (3, 1, 1, 3)$. A constant-sign edge construction in Supplementary Note "Binary constructions and complete restricted classifications" realizes the B target using $L^3/2$ vacancies. Independently, $x_x(s) = (1, 1, 0, 0)$, with other components zero, gives the required A sequence because its A count is $a_s + 2a_{s+1} + a_{s+2}$. This second realization has the same vacancy number.

At $k = (\pi/2, \pi/2, \pi/2)$, uniform f_B has zero amplitude but the prescribed f_A has a nonzero amplitude. The relation $F_A = \sqrt{2}F_B$ is violated. There is no common real solution and hence no common binary one. Direct matrix checks give $\operatorname{rank} C = 108$ and $\operatorname{rank}[C|f] = 109$. This example tests joint feasibility rather than merely the integrated counts in (S2).

Supplementary Note: Complete finite-support kernel

Laurent representation

Use $z_j = e^{ik_j}$ and the Fourier coefficients based at n rather than the physical oxygen centre. The rows are $1 + z_j^{-1}$ and $(1 + z_k)(1 + z_l)$. With the invertible change $X_j = z_j Y_j$ the matrix becomes

$$M = \begin{pmatrix} 1+z_x & 1+z_y & 1+z_z \\ z_x(1+z_y)(1+z_z) & z_y(1+z_x)(1+z_z) & z_z(1+z_x)(1+z_y) \end{pmatrix}. \tag{S7}$$

Its row cross product is $g = (g_x, g_y, g_z)$, where

$$\begin{aligned} g_x &= (1+z_x)(z_z - z_y)(1 - z_y z_z), \\ g_y &= (1+z_y)(z_x - z_z)(1 - z_x z_z), \\ g_z &= (1+z_z)(z_y - z_x)(1 - z_x z_y). \end{aligned} \tag{S8}$$

The physical anchor-basis generator is $G_j = z_j g_j$. Each component has eight signed monomials, giving 24 oxygen sites, twelve of each sign. With the convention $e^{-ik\cdot n}$, a monomial z^p is placed at $n = -p$ in the real-space stencil.

Completeness proof

Let $R_Z = \mathbb{Z}[z_x^{\pm1}, z_y^{\pm1}, z_z^{\pm1}]$. Over its fraction field, M has rank two, so its kernel is generated by g. The displayed binomial factors in (S8) have no common non-unit irreducible factor across all three components, and their integer coefficient contents are one. Thus g is primitive in this unique-factorization domain.

For any $v \in \ker_{R_Z} M$, write $v = qg$ in the fraction field and put $q = a/b$ in lowest terms. Every irreducible divisor of b would have to divide all three g_j, including its multiplicity, because b divides a g_j and is coprime to a. Primitivity forces b to be a unit. Therefore $q \in R_Z$ and

$$\ker_{R_Z} M = R_Z g. \tag{S9}$$

The same argument in the real-coefficient Laurent ring establishes completeness for arbitrary real finite-support changes. The transforms between M and C are invertible Laurent units and basis gauges, so the conclusion applies to the original neighbour operator.

The cross product vanishes exactly where all 2×2 minors vanish. Therefore $G(k) = 0$ exactly on Σ, and away from Σ it spans the one-dimensional kernel. Completeness matters here: a chosen kernel vector that happens to vanish would not, on its own, establish a failure of all compact generators. Periodic framework and flat-band work provides the mathematical context for this distinction [8,9,10].

Signed generation versus a legal binary step

A Laurent coefficient can have either sign. Equation (S9) is a complete statement about signed variations, not about paths of binary occupations. In particular, the positive support of the 24-site G stencil has some B counts equal to two and some A counts equal to three. It cannot be directly embedded as the vacancy subset of a uniform $f_B = 1, f_A = 2$ state. Combinations of translates must still be checked against a background and site capacity. The distinction between algebraic kernel generation and connectivity in constrained integer fibres is also central in the Markov-basis setting [11]. The capacity argument below avoids choosing a restricted list of executable stencils.

Supplementary Note: Periodic decomposition and dimensions

Let T be a nonsingular integer translation matrix. Its $N = |detT|$ parent cells have characters

$$\Omega_T = \{k \pmod{2\pi Z^3} : T^T k \in 2\pi Z^3\}. \tag{S10}$$

Let $K_T = \ker C_T$. Define U_T as the span of periodic images of all finite-support kernel variations of the infinite parent network. By (S9), $U_T = \operatorname{im} G_T$, where the columns of G_T are the translates of the periodized stencil. This definition of local is independent of whether an array has finitely many entries on a finite torus.

At a non-singular character, G spans the entire one-dimensional kernel. At a singular character its image is zero. Orthogonality of distinct characters therefore gives

$$K_T = U_T \oplus N_T, \qquad N_T = \bigoplus_{k \in \Sigma \cap \Omega_T} \ker C(k). \tag{S11}$$

The expression is written over complex Fourier fibres with the reality condition understood. A conjugate pair contributes the same total real dimension as its complex fibre count, not twice that count.

For $T = LI$ with even L, four diagonal lines each contain L points and meet only at Γ and R, giving 4L-6 points. Three edge lines contain 3L-2 points and intersect the diagonals only at R. Thus $|\Sigma_L| = 7L - 9$. One point has rank zero and the remaining 7L-10 have rank one. Consequently

$$\begin{aligned}\dim U_L &= L^3 - 7L + 9,\\ \dim N_L &= 2(7L - 10) + 3 = 14L - 17,\\ \dim K_L &= L^3 + 7L - 8.\end{aligned} \tag{S12}$$

For odd L no π-coordinate is sampled. The four diagonals meet only at Γ, giving 4L-3 rank-one points. Therefore

$$\dim U_L = L^3 - 4L + 3, \quad \dim N_L = 8L - 6, \quad \dim K_L = L^3 + 4L - 3. \tag{S13}$$

The cubic dimension formulas are not used for non-cubic experimental supercells. Equation (S11) is the relevant general statement. For example, the Pbam unit in Supplementary Note "Pbam coordinate mappings and registry constructions" has four characters, of which two are singular and two regular.

A periodic whole-layer switch can lie in N_T despite occupying a finite array on the torus. Cutting that switch into a bounded patch on the infinite parent creates boundary defects. Omitting these defects would conflate periodization with finite support.

Supplementary Note: Binary constructions and complete restricted classifications

Uniform five/ten coordination

The equations $f_B = 1$,$f_A = 2$ imply $\sum_i x_i = N/2$ by (S2). For a cubic binary torus L must therefore be even. This arithmetic condition concerns the uniform $ABO_{2.5}$ fibre, not the existence of the linear kernel at odd L.

For even L and arbitrary $H_z \in \{-1, +1\}$,

$$x_x(n) = \tfrac{1}{2}[1 + (-1)^{n_x+n_y} H_{n_z}], \qquad x_y = x_z = 0 \tag{S14}$$

is binary. Along x, the two B-neighbour contributions sum to one. For A, the two y-related contributions cancel their checkerboard part at each of two z positions, leaving two. Thus it has uniform BO_5/AO_{10}. Its Fourier support is contained in Γ and the line (π, π, k_z). Replacing x by y gives the second component on that edge. Axis permutations give the other edges.

For the diagonal construction let $s = n_x + n_y + n_z \bmod L$, choose $p \in \{0, 1\}$, and set $r_p(s) = 1$ when s has parity p, zero otherwise. On each active layer choose $q_s \in \{x, y, z\}$, and define

$$x_j(n) = r_p(s)\, 1_{q_s=j}. \tag{S15}$$

Then $f_B = r_p(s) + r_p(s - 1) = 1$ and $f_A = r_p(s) + 2r_p(s + 1) + r_p(s + 2) = 2$. The coordinate sum puts its Fourier support on a body diagonal. Reflection gives the other signed diagonals. If a reflected positive oxygen edge becomes a negative edge, its new anchor must be shifted by minus the corresponding unit vector; reflecting only the integer label without this anchor change is incorrect.

Complete pure-orientation classification

Assume $x_y = x_z = 0$ and require a binary solution with $f_B = 1$,$f_A = 2$. The B equation forces

$$x_x(n) = \tfrac{1}{2}[1 + (-1)^{n_x} h(n_y, n_z)], \qquad h \in \{-1, +1\}.$$

The A equation reduces to $(1 + T_y)(1 + T_z)h = 0$, where $T_j h(n) = h(n + e_j)$. Put $g(y, z) = (-1)^{y+z} h(y, z)$. Then

$$g(y, z) - g(y + 1, z) - g(y, z + 1) + g(y + 1, z + 1) = 0. \tag{S16}$$

Summing this mixed difference over a rectangle gives $g(y, z) = a(y) + b(z)$. If $a(y1) - a(y2) \neq 0$, the same nonzero difference occurs at every z. Since both values of g lie in {-1,+1}, that difference is ± 2, forcing the two rows to be constant and hence b constant. If b is nonconstant, the same argument forces a constant. Therefore g depends on only one coordinate.

Reversing the change of variables shows that all solutions are (S14), or

$$x_x(n) = \tfrac{1}{2}[1 + (-1)^{n_x + n_z} J_{n_y}]. \tag{S17}$$

The converse follows by direct substitution. Each family has 2^L members, and their intersection is the two fully staggered patterns. A fixed vacancy orientation therefore has $2^{L+1} - 2$ solutions. The three orientations have disjoint vacancy supports, giving $3(2^{L+1} - 2)$ labelled configurations.

Complete diagonal-invariant classification

Assume $x_j(n) = a_j(s)$, with binary a_j. Define $r(s) = \sum_j a_j(s)$. The B equation becomes $r(s) + r(s - 1) = 1$. Non-negative integrality forces r to alternate between zero and one. At an active layer exactly one a_j is one; the other two are zero. The A equation is then automatic, as in (S15). This proves that (S15) is the complete solution in this subspace. There are $2 \cdot 3^{L/2}$ labelled configurations.

Infinite and odd-period variants

The proofs use local differences, so arbitrary doubly infinite layer words are allowed on Z^3. No square-summability or Fourier transform of an infinite background is needed. The corresponding adjoint stencil equation $G^T x = 0$ follows directly: the checkerboard cancels an alternating factor for edge words, and equal layer dependence cancels the relevant difference factors for diagonal words.

For odd L, the uniform $\mathrm{ABO}_{2.5}$ binary fibre is empty because $N/2$ is not an integer. A useful algebraic realization of the diagonal sector instead uses ABO2: on each s-layer choose exactly one of x_x, x_y, x_z to equal one. Then $f_B = 2$ and $f_A = 4$, giving BO4/AO8. Layer orientation differences cover the two diagonal kernel directions, and the four diagonals span the odd-period nonlocal sector. This is not used as an additional material claim in the main text.

Supplementary Note: Capacity rigidity, dual criterion and nonlocal saturation

Occupancy identity

Define

$$\mathcal{P}_L = \{x \in [0,1]^{3N} : Cx = (\mathbf{1}, 2\mathbf{1})\}, \qquad \mathcal{S}_L = \mathcal{P}_L \cap \{0,1\}^{3N}. \tag{S18}$$

The constant c=1/6·1 belongs to the affine solution set. Every v∈ker C has Σv=0, so c is orthogonal to the kernel. With the unique decomposition x=c+u+ν from (S11),

$$\begin{aligned} \|u\|^2 + \|\nu\|^2 &= \|x - c\|^2 = \sum_i x_i^2 - N/12, \\ \|u\|^2 + \|\nu\|^2 + \sum_i x_i(1 - x_i) &= 5N/12. \end{aligned} \tag{S19}$$

The last term is a non-negative capacity term. It is zero exactly at a binary point and is not assigned a thermodynamic interpretation.

Rigidity of the singular binary sector

Let

$$E_L = \{x \in \mathcal{S}_L : G_L^T x = 0\}. \tag{S20}$$

Because $c \perp U_L$, this is exactly the binary sector with $u = 0$. All constructions (S14)–(S15) belong to it.

Theorem S5.1. If $x^0 \in E_L$, then $(x^0 + U_L) \cap [0,1]^{3N} = \{x^0\}$.

Proof. Let $\delta \in U_L$ and suppose $x^0 + \delta$ remains in the cube. Orthogonality gives $\langle x^0, \delta\rangle = 0$; conservation gives $\sum_i \delta_i = 0$. At sites with $x_i^0 = 1$, $\delta_i \le 0$. Their sum is exactly $\langle x^0,\delta\rangle$ and hence each is zero. At sites with $x_i^0 = 0$, $\delta_i \ge 0$, and conservation forces each of these to vanish as well. Alternatively, $\|x^0+\delta\|^2 = N/2+\|\delta\|^2$, whereas capacity and conservation imply $\|x^0 + \delta\|^2 \le \sum_i (x_i^0 + \delta_i) = N/2$. Both arguments give $\delta = 0$. □

On an infinite background satisfying $G^T x^0 = 0$, every finite-support zero mode has $\delta = Gq$ by Supplementary Note "Complete finite-support kernel". The pairing $\langle x^0, \delta\rangle = \langle G^T x^0, q\rangle$ is a finite sum and equals zero. Conservation follows from summing $C_B\delta$. The same sign argument proves rigidity even if the modified state loses periodicity.

This theorem permits any finite-support signed kernel variation, not just a selected elementary-move set. It is therefore stronger than the absence of one chosen binary flip.

General necessary and sufficient capacity criterion

For a binary $x \in \mathcal{S}_L$ set $s_i = 2x_i - 1$ and define the inward tangent orthant $T_x = \{v : s_i v_i \le 0 \text{ for every } i\}$. The following are equivalent:

(a) $(x + U_L) \cap [0,1]^{3N} = \{x\}$;

(b) $U_L \cap T_x = \{0\}$;

(c) there is $w \in U_L^\perp$ with $s_i w_i > 0$ for every i.

Proof. The equivalence of (a) and (b) follows by scaling a non-zero tangent direction and, conversely, taking the difference of two feasible occupations. For (c)⇒(b), every nonzero $v \in T_x$ has $\langle w, v\rangle < 0$, contradicting $v \in U_L$.

For (b)⇒(c), project the orthant generators $-s_i e_i$ onto $U_L^\perp$. If zero lay in their convex hull, a nonzero non-negative combination of the original generators would lie in $U_L \cap T_x$. The generators are distinct coordinate directions, so such a combination cannot itself be zero. This contradicts (b). Strict separation of the finite convex hull from zero gives a vector $w \in U_L^\perp$ with $\langle w, -s_i e_i\rangle < 0$ for all i, proving (c).

Since $U_L \subset \ker C_L$,

$$U_L^\perp = \operatorname{im} C_L^T \oplus N_L. \tag{S21}$$

The separating weights can therefore be decomposed into coordination weights and nonlocal weights. For E_L one can simply use $w = 2x - 1$. The criterion concerns absence of any second capacity-allowed point; it does not classify every disconnected pair of binary states when fractional motion is possible.

Complete binary saturation

Theorem S5.2. For even L, $\operatorname{span}_{\mathbb{R}}(E_L - E_L) = N_L$.

Proof. Every difference belongs to N_L by (S20). For the reverse inclusion, consider changes of the orientation of one active diagonal layer in (S15). The two parity choices allow the layer to be any s, and two independent exchanges give the component differences $e_y - e_x$ and $e_z - e_x$. Translates and linear combinations give arbitrary profiles of these two directions along the corresponding diagonal. At each non-R diagonal character they span its two-dimensional kernel, including the two-dimensional zero-sum kernel at Γ. Correctly reflected constructions give the other diagonals.

On the edge (π, π, k_z), a single H_z flip in (S14) gives an arbitrary layer profile in the x component. Its y-oriented counterpart gives the second edge component. These span the two-dimensional kernel at rank-one edge points away from R. At R the three edge orientations supply e_x, e_y, e_z, which span its full three-dimensional kernel. Thus every singular fibre is covered. Fourier projection is legitimate because the real span of all translated construction differences is translation invariant; conjugate fibres combine to real vectors. □

This is a linear-span realization of the entire nonlocal sector. A prescribed arbitrary real vector in N_L need not itself be a difference of a single binary pair.

Supplementary Note: Hidden-coordinate geometry, counting and structural distance

Let $H_L = P_{N_L}(\mathcal{P}_L - c)$ and $R_L^2 = 5N/12$. Equation (S19) implies H_L is contained in the closed ball of radius R_L. A point ν reaches the sphere if and only if its preimage is binary and $u = 0$. Hence sphere-contact points are exactly $x - c$ with $x \in E_L$, and each has the unique preimage $c + \nu$.

For a contact point ν^0, Cauchy–Schwarz gives $\langle \nu^0, \nu\rangle \le R_L^2$ on all H_L. Equality requires $\nu = \nu^0$. Thus every contact point is an exposed point of this projected polytope. This is a geometric property of the occupancy constraints, not an energy landscape.

If $x, y \in E_L$, then $x - y = \nu_x - \nu_y$ and

$$d_H(x, y) = \|x - y\|^2 = \|\nu_x - \nu_y\|^2. \tag{S22}$$

This is a squared-Euclidean representation of Hamming distance; equivalently $\sqrt{d_H}$ is the Euclidean distance after embedding. For arbitrary binary x,y in the same hidden-coordinate class ν, their local components have common squared norm $R_L^2 - \|\nu\|^2$, so

$$d_H(x, y) \leq 4(R_L^2 - \|\nu\|^2). \tag{S23}$$

No connectivity assumption enters this diameter bound. For a rigid reference $x^0 = c + \nu^0$ and any $y \in \mathcal{P}_L$, capacity and fixed total vacancy count give

$$\|y - x^0\|_1 = 2\langle \nu^0, \nu^0 - \nu_y \rangle. \tag{S24}$$

Indeed, the left side equals $2(N/2 - \langle x^0, y \rangle)$, and $\langle x^0, y \rangle = N/12 + \langle \nu^0, \nu_y \rangle$.

Number of rigid configurations

The edge family gives at least 2^L points of E_L. A d-dimensional affine subspace intersects the binary cube in at most 2^d vertices: select d coordinate functionals that are independent on its direction space, giving an injective projection into d binary coordinates. Since $E_L \subset c + N_L$,

$$2^L \leq |E_L| \leq 2^{14L-17}. \tag{S25}$$

Therefore $\log |E_L| = \Theta(L)$. Dividing by a parent symmetry group of size at most $48L^3$ cannot change this exponential order. This counts configurations, not an equilibrium statistical ensemble.

Exact pure-orientation orbit count

Under the complete parent group, the union of the three pure-orientation families reduces to length-L binary words modulo cyclic shift, reversal and sign complementation. Axis permutations choose a standard vacancy orientation and stacking axis. Operations preserving these act as the stated word transformations. A swap between the two transverse axes can identify the two normal forms only when both words are fully staggered; those are already identified by complementation. Thus there are no further generic identifications.

Burnside's lemma gives, for even L,

$$b_L = \frac{1}{4L}\left[\sum_{r=0}^{L-1} 2^{\gcd(L,r)}\left(1 + 1_{L/\gcd(L,r) \text{ even}}\right) + L\, 2^{L/2+1}\right]. \tag{S26}$$

A shift r has $\gcd(L, r)$ cycles. With complementation, fixed words exist only when each cycle length is even. Of the L reflections, half have two fixed positions and half have none; adding their complemented versions gives the displayed reflection term. The first four counts are $b_2 = 2, b_4 = 4, b_6 = 8, b_8 = 18$. All non-identity rotations have at most L/2 cycles, so $b_L = 2^L/(4L) + O(2^{L/2})$.

Minimum separation of the pure-orientation family

For two words in the same orientation and stacking branch, $d_H = L^2 d_{\mathrm{word}}$, so one-letter change attains L^2. For two branches with the same vacancy orientation, define $u_z = (-1)^z H_z$ and $v_y = (-1)^y J_y$. If a,b are their numbers of positive entries,

$$d_H = L[a(L-b) + (L-a)b]. \tag{S27}$$

When nonzero, the bracket is at least L: at b=0,L this is direct, and for $0 < b < L$ the linear expression in a has its minimum at an endpoint. Different vacancy orientations have disjoint vacancy supports, giving distance L^3. Thus the minimum nonzero distance over the whole pure-orientation union is L^2.

The supplied L=4 binary counterexample with nonzero regular content further shows E_L is not the entire fibre $\mathcal{S}_L$. Its decomposition is $\|u\|^2 = 19/2$ and $\|\nu\|^2 = 103/6$. It is preserved as a checked counterexample, not used to infer the existence of an executable binary local path.

Supplementary Note: Domain restriction and defect moments

A general domain-restriction identity

Let x^0, x^1 be binary configurations with $Cx^0 = Cx^1 = f$ and $\delta = x^1 - x^0$. For oxygen masks $\eta_o \in [0,1]$, put $y = x^0 + \eta_o \delta$. For any cation masks η_c,

$$(Cy - f)_c = \sum_o C_{co}(\eta_o - \eta_c)\delta_o. \tag{S28}$$

To prove this, start from $Cy - f = C(\eta_o \delta)$ and subtract $\eta_c \sum_o C_{co}\delta_o = 0$. If the mask is constant on all changed oxygen neighbours of a cation, its defect vanishes. Hence only the neighbour-thick interface may contribute; terms there may also cancel. For binary masks, y chooses one binary endpoint at each site. Vacancy-number conservation is the additional condition $\sum_o \eta_o \delta_o = 0$.

In operator notation this is $(CM_\eta^O - M_\eta^c C)\delta$. The multiplication operators act on different spaces; the expression is not an undefined square-matrix commutator. If x^0 is a rigid infinite background and $\eta\delta$ is a nonzero finite change, its defect cannot vanish everywhere by Theorem S5.1. The identity also describes aligned extended interfaces with cancellation, so it does not assert that every interface between different decorations must be defective.

Vacancy transfer and coordination-defect moments

Take any finite-support signed change δx on the infinite parent. Define $d = C\delta x$, $T_j = \sum_n \delta x_j(n)$, and $T = \sum_j T_j$. Form the signed coordination-count measure

$$\rho = \sum_n d_A(n)\,\delta_{n+a} - 2\sum_n d_B(n)\,\delta_n. \tag{S29}$$

For one j-oriented oxygen edge with centre r, the B positions are $r \pm e_j/2$ and the A positions are $r \pm e_k/2 \pm e_l/2$. Their zeroth and first sums cancel in (S29). Their second sums give

$$\sum_A rr^T - 2\sum_B rr^T = I - 2e_j e_j^T$$

for that edge's contribution. Summing with the coefficients δx yields

$$\int \rho = 0, \qquad \int r\rho = 0, \qquad Q := \int rr^T\rho = TI - 2\,\mathrm{diag}(T_x, T_y, T_z). \tag{S30}$$

The zero lower moments make Q independent of a common origin. For $T = 0$, Q is traceless, $Q_{ij} = 0$ for $i \neq j$, and $T_j = -Q_{jj}/2$. Thus finite exact coordination-preserving changes conserve the vacancy number of each orientation separately.

A binary example starts from the edge background with H=+1. Take $\delta x_x(0) = -1$ and $\delta x_y(0) = +1$. The nonzero B defects are $d_B(e_x) = -1$ and $d_B(e_y) = +1$. The A defects are +1 at -e_x and $-e_x - e_z$, and -1 at -e_y and $-e_y - e_z$. Therefore $T = (-1, +1, 0)$ in orientation components and $Q = \mathrm{diag}(2, -2, 0)$. The example remains a binary occupation with the same total vacancy number but has left the uniform coordination fibre.

At R define $\chi(n) = (-1)^{n_x+n_y+n_z}$ and $S_j = \sum_n \chi(n)\delta x_j(n)$. The two B endpoints of an oxygen edge have opposite χ. Direct endpoint summation gives

$$\sum_n \chi(n)d_B(n) = 0, \qquad S_j = -\sum_n n_j\chi(n)d_B(n). \tag{S31}$$

Under a signed axis permutation, edge-anchor relabelling makes this staggered triplet transform as a vector. At Γ, the orientation redistribution with $T = 0$ transforms as a traceless diagonal tensor. The different representations agree with the different moment orders below.

Complete singular-amplitude reconstruction from defect derivatives

Because δx has finite support, its Fourier transform and those of its defects are finite exponential sums. They can be differentiated with respect to continuous k. Write X for the transform of δx and F_A,F_B for its defects. The following reconstruct all three oxygen amplitudes at every point of Σ.

At Γ,

$$X_i(0) = \frac{F_B(0)}{4} + \frac{\partial_i^2 F_A(0) - 2\partial_i^2 F_B(0)}{2}. \tag{S32}$$

Indeed, $C_A - 2C_B$ and its first derivatives vanish at Γ. Its second ii derivative is $2e_i^T - 1^T$. The derivative combination is therefore $2X_i - \sum_j X_j$, and $F_B = 2\sum_j X_j$. This proves (S32) and reproduces (S30).

At $k = (\varepsilon_x t, \varepsilon_y t, \varepsilon_z t)$ with $\varepsilon_i = \pm 1$ and $0 < t < \pi$, set $c = \cos(t/2)$, $s = \sin(t/2)$. Then

$$X_i(k) = \frac{F_B(k)}{4c} + \frac{\partial_i F_A(k) - 2c\,\partial_i F_B(k)}{4\varepsilon_i cs}. \tag{S33}$$

Here 2c is evaluated at the chosen point and is held fixed in the derivative combination. The identity $C_A = 2cC_B$ cancels all unknown derivatives of X. Differentiating the rows gives $\partial_i F_A - 2c\partial_i F_B = 2\varepsilon_i cs(2X_i - \sum_j X_j)$, from which (S33) follows.

On the edge k=(π,π,t), $c = \cos(t/2) \neq 0$,

$$X_x = -\frac{\partial_y F_A}{2c}, \qquad X_y = -\frac{\partial_x F_A}{2c}, \qquad X_z = \frac{F_B}{2c}. \tag{S34}$$

Here $C_A = 0$ and its x,y derivatives select the opposite transverse oxygen component. Cyclic permutation gives the other two edges. Finally, at the representative $R = (\pi, \pi, \pi)$,

$$X_i(R) = -\partial_i F_B(R), \tag{S35}$$

because $C_B = 0$ and $\partial_i C_B = -e_i^T$. Equivalent zone-boundary representatives require the basis phases from (S3).

The special Γ and R formulas replace, rather than regularize, the divisions by zero in the interior formulas. They complete the singular set.

Second order at Γ is genuinely necessary on the space of finite signed changes. Choose δx_x at n=0 and -e_x equal to +1 and δx_y at n=0 and -e_y equal to -1. Then $X = (2c_x, -2c_y, 0)$, $F_A = 0$ and $F_B = 2(\cos k_x - \cos k_y)$. Both defect fields and all their first derivatives vanish at Γ, although $X(0) = (2, -2, 0)$. This is an algebraic counterexample to reconstruction from first-order data alone; no embedding of this particular signed pattern in a uniform binary background is needed for the claim.

At Γ, the scalar coordination output cannot carry the two-dimensional traceless orientation representation, and a first-order vector does not contain it. Second-order moments do. At R, the staggered first moments already match the hidden triplet. The explicit formulas supply the full argument in this lattice, rather than relying only on representation labels.

A finite-change identity at a rigid background

Let x^0 be an L-periodic member of E_L, and let $y = x^0 + \delta x$ be capacity allowed on the infinite lattice, with δx finite. Use unnormalized Fourier amplitudes $X^0(k)$ over one background period, and let $J_k[d]$ denote (S32)–(S35). Binary x^0 gives $|\delta x_i| = (1 - 2x_i^0)\delta x_i$ at every site. Fourier expansion of the periodic background therefore yields

$$\|\delta x\|_1 = T - \frac{2}{L^3} \operatorname{Re} \sum_{k \in \Sigma_L} X^0(k)^\dagger J_k[d]. \tag{S36}$$

All boundary defects of δx must be included. If d vanishes identically, every jet vanishes, conservation gives $T = 0$, and the identity recovers rigidity. The formula uses phase-sensitive defect fields and spatial moments, not intensity-only diffraction data. The coordinates are parent reference coordinates; actual distorted positions require their own moment derivation.

Supplementary Note: Complete single-layer channel and exact switching extremum

Complete state parametrization

Fix even $L \geq 4$ and an $L \times L \times L$ parent torus. In z=0 take the x-oriented edge state $x_x^0(x, y, 0) = [1 + \chi(x, y)]/2$, $\chi = (-1)^{x+y}$. Other layers remain fixed. Any binary change confined to these oxygen sites is uniquely

$$\delta x_x(x,y,z) = -\chi(x,y)\eta(x,y)1_{z=0}, \quad \eta \in \{0,1\}^{L\times L}. \tag{S37}$$

Vacancy number is conserved if and only if $\sum \chi\eta = 0$. The target whole-layer switch is η=0 to η=1.

Direct substitution in (S1) gives

$$\begin{aligned} d_B(x,y,z) &= -\chi[\eta(x,y) - \eta(x-1,y)]1_{z=0}, \\ d_A(x,y,z) &= -\chi[\eta(x,y) - \eta(x,y+1)](1_{z=0} + 1_{z=-1}). \end{aligned} \tag{S38}$$

Each nonzero defect has amplitude one. With

$$b_x = \sum |\eta(x,y) - \eta(x-1,y)|, \quad b_y = \sum |\eta(x,y) - \eta(x,y+1)|,$$

we have $D_B = b_x$, $D_A = 2b_y$ and $D_B + D_A/2 = |\partial\eta|$. The two A layers account for the factor two. Interior flipped sites remain in the same coordination field; the defects trace the boundary.

Allowed elementary steps

An elementary step exchanges occupied and vacant x-oriented oxygen sites at neighbouring (x,y) coordinates in this layer. Since neighbouring χ values have opposite signs, their occupations differ exactly when their η values are equal. Thus a legal exchange is precisely a dimer toggle 00↔11 on an adjacent pair. It preserves $\Sigma\chi\ \eta$ and changes $|\eta|$ by ±2. A pair with η=01 or 10 has equal physical occupations and is not a non-trivial exchange.

This specifies the entire channel, including backwards and non-monotone paths. No assumption that a path must scan rows enters the lower bound.

Necessary perimeter and equality cases

Any path from area zero to L^2 crosses area $L^2/2$, because all areas are even and each step changes them by two. For a half-area mask on the periodic square, $|\partial\eta| \geq 2L$. To prove this, if there are both a full row and an empty row, every column has at least two vertical transitions. If all rows are mixed, every row has at least two horizontal transitions. In the remaining case, after possibly taking the complement there is an empty row and no full row. If m rows and n columns are nonempty, every nonempty row and column is mixed. Therefore $|\partial\eta| \geq 2m + 2n \geq 4\sqrt{mn} \geq 2\sqrt{2}L > 2L$.

Equality in the first case requires zero horizontal boundary, so every row is constant; exactly two vertical transitions then force a consecutive half-width horizontal strip. Equality in the second case requires zero vertical boundary, giving its vertical counterpart. Hence the only equality masks are straight half-width strips.

For such a strip, an allowed dimer lies wholly in either value of η. Its toggle changes the six external incident edges; if q of those edges were already on the strip boundary, $\Delta|\partial\eta| = 6 - 2q$. Since the strip and its complement both have width L/2≥2, q≤2 for an allowed dimer. Thus every legal neighbour of a minimum strip has perimeter at least 2L+2. A non-minimum half-area mask also has perimeter at least 2L+2 because perimeter is even. Every switching path therefore reaches 2L+2.

Attaining construction and single-field optima

Scan rows y=0,...,L-1. In each row exchange the disjoint pairs x=0/1,2/3,...,L-2/L-1. Each pair initially has opposite occupation, and no pair is reused. Every intermediate mask consists of completed rows plus an even-length prefix in the next row. Its horizontal boundary is at most two and its vertical boundary at most 2L. The maximal perimeter is 2L+2. Exactly $L^2/2$ exchanges are used, the minimum possible because the endpoints differ on L^2 oxygen sites.

The transposed column scan has $b_y \le 2$ and $b_x \le 2L$. Therefore the two scans achieve, respectively,

$$\max D_B = 2,\ \max D_A = 4L; \qquad \max D_B = 2L,\ \max D_A = 4. \tag{S39}$$

The first non-trivial exchange in any path creates at least two B defects and at least four A defects: two distinct parallel oxygen edges have at most one common B endpoint, and nearest-neighbour edges along y have at most two common A neighbours. Hence these separate lower bounds are attained by the two scans. Combining with the perimeter proof,

$$\inf_\gamma \max D_B = 2, \quad \inf_\gamma \max D_A = 4, \quad \inf_\gamma \max(D_B + D_A/2) = 2L + 2. \tag{S40}$$

The path set is the same in all three optimizations. The different objectives need not have the same optimizer. The unweighted total also has $2L \le \inf_\gamma \max(D_B + D_A) \le 2L + 4$. These statements concern coordination-defect measures. They do not provide a migration energy or extend the lower bound to paths using other layers and orientations.

The perimeter value $2L + 2$ has close analogues in communication-height results for periodic Ising/Potts models [19,20]; the update graph and physical defect variables here are different, and the derivation is retained for completeness.

Necessary and sufficient inverse defect conditions

Suppose integer candidate defects have the support in (S38), with identical A arrays on z=0 and -1. Put $b = -\chi d_B$ and $a = -\chi d_A$ on z=0, then define $p(x, y) = b(x + 1, y)$ and $q(x, y) = -a(x, y)$. They must be the forward x and y differences of η.

They integrate to a periodic integer potential v if and only if their elementary plaquette curl vanishes and both independent torus circulation sums are zero:

$$p(x, y + 1) - p(x, y) = q(x + 1, y) - q(x, y), \quad \sum_x p(x, y) = 0, \quad \sum_y q(x, y) = 0. \tag{S41}$$

Necessity follows by telescoping. Sufficiency follows by integrating along paths: curl zero makes contractible detours irrelevant, and zero circulations remove the two non-contractible detours. Normalize $v(0, 0) = 0$. A binary realization exists precisely when $\max v - \min v \le 1$. A number-conserving realization additionally requires $\sum \chi(v - \min v) = 0$. Nonzero defects imply width one and uniquely give $\eta = v - \min v$. Zero defects have the two constant solutions η=0,1, both number conserving for even L.

Linear integrability is not sufficient for binary feasibility. At L=4 take $v = (0, 1, 2, 1)$ along x, constant along y. Its gradient is periodic, curl free and has entries 0 or ± 1, but its width is two. Thus even small individually plausible defect amplitudes can fail occupancy capacity.

Supplementary Note: Pbam coordinate mappings and registry constructions

Sources and assignment

The Ca structure is the Rietveld refinement in Table S1 accompanying Kim et al. [12]. We consistently use the lattice constants in that table, including $b = 10.2322$ Å. The Sr structure is Caignaert et al. [2], obtained from COD entry 1001352, revision 130149. Supplementary Table S1 records the independent positions used. These are published experimental coordinate models, not structures optimized in this work.

Expand the following Pbam operations modulo one:

(x,y,z), (-x,-y,z), (x+1/2,-y+1/2,-z), (-x+1/2,y+1/2,-z), (-x,-y,-z), (x,y,-z), (-x+1/2,y+1/2,z), (x+1/2,-y+1/2,z).

Duplicate positions on special sites are removed. Each model has four A, four B and ten occupied oxygen positions. With

$$S = \begin{pmatrix} 1 & 2 & 0 \\ 1 & -2 & 0 \\ 0 & 0 & 1 \end{pmatrix}, \quad o = (1/2, 0, 0), \quad p = Sf - o, \tag{S42}$$

the B sites assign to integer parent vertices and A sites to integer labels plus a. The twelve candidate oxygen sites are all three positive parent edges from four B translation classes. Minimum periodic distances in the reported orthorhombic metric give a one-to-one oxygen assignment. In both materials each assigned oxygen is also its individual nearest candidate; no occupancy conflict must be resolved by selecting a more distant site.

The unoccupied edges are Y at r=0 and X at r=3, where $r = n_y - n_x \bmod 4$. Representatives are y at n=0 and x at n=(1,0,0). The maximum oxygen displacement and smallest assignment gap are listed in Table S2. Direct full-neighbour evaluation gives $f_B = 1$ and $f_A = 2$ everywhere.

Spectral decomposition on the experimental cell

The character group of S has representatives Γ, (π,π,0) and $\pm(\pi/2, -\pi/2, 0)$. The first two are singular. The latter two are regular rank-two points. Center the vacancy pattern by c=1/6 and take a unitary transform over the four parent cells. Summing squared vector amplitudes over these sets gives

$$\|u\|^2 = 1, \qquad \|\nu\|^2 = 2/3, \quad \|u\|^2 + \|\nu\|^2 = 5/3. \tag{S43}$$

An equivalent $4 \times 4 \times 1$ torus contains four copies of the Pbam unit; its total norms must be divided by four to report (S43). These structures have nonzero regular content and are not members of E_L. The regular part being in the signed local span does not by itself prove a legal binary local path from the experimental decoration.

Complete reality-derived stripe classification

Retain invariance along (1,1,0) and e_z, allow only x and y vacancies, and set $X_r = x_x(n), Y_r = x_y(n)$ with $r = n_y - n_x$. Equation (S1) gives

$$f_B(r) = X_r + X_{r+1} + Y_r + Y_{r-1}, \qquad f_A(r) = 2f_B(r). \tag{S44}$$

Between registry vertices r and r+1, the two possible physical vacancy edges are Y_r and X_{r+1}. Uniform $f_B = 1$ requires that each vertex be incident to exactly one chosen edge. On an even cycle of length $m \geq 4$, the underlying matching has one of two parities, and each matched pair has two independent labels. Therefore all solutions are obtained by this construction and

$$N_m = 2^{m/2+1}. \tag{S45}$$

For m=4, $N_4 = 8$. For m=8, $N_8 = 32$; exactly eight are invariant under a registry translation of four. The other 24 have primitive registry period eight. These are labelled configurations in this subspace, not 24 symmetry-inequivalent or experimentally resolved phases.

The new enlarged domains and stacking faults in the HREM study [3] motivate this subspace. The count provides admissible candidates of the reported type; the bulk model and accessible defect-class descriptions do not assign a unique candidate to each micrograph.

Registry changes and matching parity

Let the four bulk translational variants have Y vacancies at r=p and X vacancies at $r = p - 1$ modulo four. A shift $p \to p + 2$ preserves the matching parity and reverses the X/Y labels. Its difference has only the two regular quarter-wave components. A shift $p \to p \pm 1$ changes the matching parity and also changes the singular component at $M_{xy} = (\pi, \pi, 0)$. Here M_{xy} is not the three-coordinate point $R = (\pi, \pi, \pi)$.

On an infinite chain, once a matched pair is chosen, a degree-one matching forces all remaining pair locations recursively. Thus a matching cannot change its parity across a finite-width interface while retaining degree one everywhere. A parity-changing interface in this stripe subspace must contain a B defect and, by (S44), an A defect. By contrast, any X/Y label sequence on one fixed pair pattern is allowed. An aligned boundary between two such sequences remains uniform BO_5/AO_{10}.

These label changes extend over the directions in which the stripe model is invariant. They are not finite-support three-dimensional moves and hence do not contradict the finite-support rigidity theorem for E_L. A vacancy-free perovskite region has $f_B = f_A = 0$ and is a different coordination fibre, distinct from a registry boundary between two uniform five/ten states.

Supplementary Note: Homologous vacancy planes and intergrowth

Reported structure and parent model

Refs. 4 and 5 establish and organize the $Sr_{4+n}Mn_{4+n}O_{10+3n}$ phases. The published microsymposium abstract [13] reports vacancy lines along the parent [001] direction within (310) planes and coherent n=1/n=3 growth at a shared plane. This is the experimental motivation for the following parent occupation rule. The plane motif is not newly assigned by our calculation; the joint A/B counting rule is derived here from it.

The nominal ordered vacancy sites in the source-derived n=1 and n=3 coordinate models agree with this parent lift. For n=1 a parent translation matrix may be taken as columns (2,1,0),(-1,2,0),(0,0,1); interchanging the first two parent axes and translating gives the motif below. For n=3 one may take columns (2,1,0),(1,-3,0),(0,0,1). Their determinants have absolute values five and seven. Table S4 lists the nominal

sites used for this correspondence. The tabulated partial oxygen occupations in the published refinements are average-site populations; the construction below uses the nominal fully vacant ordered-site model rather than assigning binary local coordinations to those averages.

Exact window identity

Define $s = t(n) = 3n_x + n_y$ and let $R \subset \mathbb{Z}$ be a locally finite set of distinct integer plane anchors, with indicator I. Set

$$x_x(n) = I(s), \quad x_y(n) = I(s-1), \quad x_z(n) = 0. \tag{S46}$$

An x vacancy at anchor r has oxygen-centre t=r+3/2. The y vacancy with parent anchor r+1 has the same centre coordinate, so the two types lie in a common (310) plane.

For B, the x terms are I(s),I(s-3), and the y terms are I(s-1),I(s-2). For A, the x terms are twice I(s)+I(s+1), and the y terms are twice I(s-1)+I(s+2). Thus, at the same labelled parent cation fields,

$$f_B(s) = \sum_{j=0}^{3} I(s-j), \qquad f_A(s) = 2\sum_{j=-1}^{2} I(s+j) = 2f_B(s+2). \tag{S47}$$

The offset s+2 is part of the site-resolved statement. Moving the A window by one layer leaves histograms unchanged but would mislabel the actual A field.

Theorem S10.1. Within (S46), the condition that $f_B \in \{0,1\}$ and $f_A \in \{0,2\}$ everywhere is equivalent to every consecutive plane spacing being at least four.

Proof. With spacings at least four, each four-integer window contains at most one anchor. Both conditions follow from (S47). Conversely, anchors at separation one, two or three lie together in some four-integer B window, giving $f_B \geq 2$. The A condition is then also violated at a shifted site. □

The theorem applies to periodic and non-periodic anchor sequences. It is a complete criterion within the two-edge plane motif, not a classification of every mixed-coordinate vacancy model at the same composition.

Uniform homologues and coordination words

For one anchor in a registry period m=n+4, the parent translation lattice has m cells and there are exactly two vacancies. Hence O/B=3-2/m and the formula is $A_{4+n}B_{4+n}O_{10+3n}$. A B window equals one on four residue classes and zero on n; the A window equals two on four classes and zero on n. Thus the counts per repeat are

$$4\,BO_5 + n\,BO_6, \qquad 4\,AO_{10} + n\,AO_{12}. \tag{S48}$$

Along e_y the registry advances by one, giving four consecutive p symbols and n o symbols, or pp o^n pp up to cyclic origin. Along e_x it advances by three. For m=7 the corresponding word is cyclically popopop, and for m=8 popoopop. These agree with the canonical paired building words in the homologous description [5].

At m=4, $t = 3n_x + n_y$ is congruent to $n_y - n_x$ modulo four. With an anchor-origin shift, (S46) is therefore the Pbam decoration mapped in Supplementary Note "Pbam coordinate mappings and registry constructions".

The step-three action on $\mathbb{Z}/m$ has $\gcd(3, m)$ cycles. At m=6 it has three two-cycles, with coordination words pp,po,po, whereas m=4,5,7,8 each has one cycle. This arithmetic fact organizes the directional registry of the canonical n=2 model. It is not a criterion for energetic instability, nor does it cover every alternative n=2 building arrangement.

Intergrowth and the n=2 average composition

Take anchors …,-10,-5,0,7,14,… . One side has the n=1 spacing five and the other the n=3 spacing seven, sharing anchor zero. Theorem S10.1 gives only BO_5/BO_6 and AO_{10}/AO_{12} throughout, including the junction. In the ideal parent lift this construction supplies a coherent, registry-matched interface with no additional coordination class. It corresponds to the geometry reported in ref. 13, rather than a reconstruction of an unavailable complete atomistic interface image.

For a periodic alternating 5/7 sequence, one period contains twelve registry cells and two motifs, hence four vacancies. It has O/B=3-4/12=8/3 and counts

$$8\,BO_5 + 4\,BO_6, \qquad 8\,AO_{10} + 4\,AO_{12}. \tag{S49}$$

A homogeneous spacing-six model has the same composition and histograms after placing it in a common twelve-period unit. Its site-resolved fields differ from those of the 5/7 arrangement. Therefore the comparison concerns compatibility and palette, not equality of the two complete coordination fibres. Both structures are allowed by (S47); energetic selection between them is additional to this construction. The experimental SrMnO2.668 value is a reported composition, while 8/3 is the exact stoichiometry of the ideal alternating model.

Partially occupied nominal vacancy sites

The n=1 model's nominal pair derives from the P4/m orbit of (1/2,0,0). For n=3 the two nominal sites are (1/2,0,0) and (1/2,1/2,0) in the stated P2/m setting. These positions map to the two parent edge families. Where the experimental refinement assigns partial oxygen occupancy, the corresponding average vacancy variable is one minus that occupancy. Applying C then gives average missing-neighbour counts. It does not establish the instantaneous binary occupancy correlations or local-valence assignment. No binary theorem in this paper is inferred merely by rounding a partially occupied average site.

Supplementary Note: Pnma $CaMnO_{2.75}$ descriptor example

A standard four-formula-unit Pnma parent has translation columns (1,0,1),(0,2,0),(-1,0,1). Its translation quotient is $\mathbb{Z}_2 \times \mathbb{Z}_2$, which can be labelled by $(n_x + n_z \bmod 2, n_y \bmod 2)$. A single oxygen vacancy per cell gives Ca4Mn4O11 and hence $CaMnO_{2.75}$.

For a y-oriented vacancy, its two B endpoints are different quotient classes, so two B sites lose one oxygen and two lose none. The four A neighbours involve shifts along x and z. These two shifts act identically on this quotient, so the four incidences collect two each on two A classes. The count sets are

$$f_B : \{0, 0, 1, 1\}, \qquad f_A : \{0, 0, 2, 2\}. \tag{S50}$$

For an x-oriented vacancy, the B endpoints again give two single deficits. Its A neighbours involve indepen-

dent y and z shifts, covering all four quotient classes once:

$$f_B : \{0, 0, 1, 1\}, \qquad f_A : \{1, 1, 1, 1\}. \tag{S51}$$

The z orientation gives the same second pattern. In the ideal standard Pnma setting, the O1 apical class is the y-edge type and the O2 equatorial class comprises x/z edges. Thus the two classes share the B coordination histogram $2BO_5$+$2BO_6$, but have $2AO_{10}$+$2AO_{12}$ and $4AO_{11}$. This is a histogram comparison; we do not assert equality of their site-labelled B fields.

Molinari et al. [14] considered two $CaMnO_{2.75}$ arrangements arising from the inequivalent oxygen positions and found different relaxed structural and transport properties, while retaining the stated five/six Mn environments. Chiang and Poeppelmeier [15] had earlier reported an inconclusive distinction between proposed structures with the same pyramid/octahedron fraction. Equations (S50)–(S51) give an additional structural descriptor, not a resolution of every historical refinement model. Without a verified correspondence between the actual input structures and figure labels in ref. 14, we do not assign the two A patterns to its zig-zag/line labels or attribute an energy splitting to A coordination alone.

Supplementary Note: Reciprocal contrast, public ideal structures and homometry

Experimental-cell reciprocal classes

For the Pbam transformation (S42), an orthorhombic reflection H=(h,k,l) maps to parent reciprocal-lattice units

$$q = S^{-T}H = (h/2 + k/4,\ h/2 - k/4,\ l). \tag{S52}$$

For even k, even h+k/2 gives the Γ class and odd h+k/2 the M_{xy} class. Odd k gives one of the two regular quarter-wave classes. The two missing parent oxygen positions in orthorhombic fractions are $v1 = (1/2, 0, 0)$, $v2 = (0, 1/2, 0)$. Relative to the fully occupied ideal parent oxygen lattice, their vacancy contrast is

$$\Delta F_{\mathrm{vac}}(hkl) = -f_O[(-1)^h + (-1)^k]. \tag{S53}$$

It is $+2f_O$ at (131) and $-2f_O$ at (061). Using the SI Table S1 cell of ref. 12 and $\lambda = 1.5406$ Å gives $2\theta = 39.3673°$ and $59.5157°$. These are calculated positions for a representative Cu Kα1 wavelength. The corresponding labels occur in the published indexed pattern. That consistency links the source refinement to the calculated reciprocal classes; it does not constitute an independent measurement of $\|u\|^2$ or $\|\nu\|^2$.

At (230) the ideal two-vacancy scalar contrast cancels although the reflection lies in a regular class. Actual occupied-oxygen and cation displacements can contribute to a superstructure reflection. Similarly, phase-sensitive vector amplitudes at equivalent reciprocal representatives must be rephased with their oxygen basis. Neither the vector norm decomposition nor the ideal vacancy contrast should be substituted for a complete refined intensity model.

Layer words and superstructure contrast

For (S14), subtract the mean x-oriented occupation 1/2. With unnormalized Fourier amplitudes on an L^3 cell,

$$X_{\mathrm{mod}}(\pi,\pi,k_z) = \frac{L^2}{2} e^{-i\pi/2} \sum_{z=0}^{L-1} H_z e^{-ik_z z}. \tag{S54}$$

This follows by summing the two transverse checkerboards. At L=4, $H = (+1,+1,+1,+1)$ gives $|X_{mod}|^2 = 1024$ at $k_z = 0$; $H = (+1,+1,-1,-1)$ gives 512 at each $k_z = \pm\pi/2$. Their full A/B coordination fields are identical. The calculation provides a forward structural contrast for their different vacancy order.

The two publicly generated ideal structures `L1_vac2_t0.67` and `L2_vac6_t1.17` from the source associated with ref. 6 map to $H = (+1,+1,+1,+1)$ and $H = (+1,-1,-1,+1)$, respectively, the latter being a cyclic shift of $(+1,+1,-1,-1)$. The coordinate mappings, rather than a coordination label in a filename, are checked against the parent network. They are ideal generated structures, separate from the experimental Pbam models. Their source snapshots and derived fields are retained with their provenance.

A phase-loss counterexample

Take two length-12 words with positive-index sets {0,1,4,6} and {0,1,3,7}, and negative entries elsewhere. They are not related by cyclic shift, reversal or global sign complementation. Their complete cyclic autocorrelations are identical, so their discrete Fourier intensities are identical. Inserting them in (S14) gives different rigid structures with the same layer-word intensity. This is an instance of the established homometry problem [16]. It demonstrates the difference between the phase-retaining coordinates ν in (S22) and an intensity-only observation. It supplies no new uniqueness assertion for powder data.

Supplementary Note: Verification, data provenance and inheritance

Independent finite checks

The proofs establish the size-general results. Computation checks the operator conventions, explicit constructions and small finite cases. The core programs assemble integer neighbour matrices and probe them with plane waves, rather than inserting the analytical symbol as the matrix. The Laurent cross product and primitive gcd are checked symbolically. Modular elimination gives rank lower bounds over the rationals/reals; agreement with independently proved upper bounds closes the tested ranks.

The supplied verification programs include:

- complete wavevector and rank checks for L=2,3,4,5,6;
- binary rigid-state construction differences at even L=2,4,6;
- complete reduced Boolean enumeration for pure-orientation and diagonal-invariant L=2,4 fields;
- complete parent-group orbit counts at L=2,4,6,8;
- finite perturbations evaluated by direct neighbour counting and independent defect-moment sums;
- all 12,870 half-area masks at L=4, followed by threshold path searches;
- row and column exchange constructions checked through every state;
- full three-dimensional counts for the homologous coordination windows, including spacing-one/two/three counterexamples;
- one-to-one Ca/Sr coordinate assignments, Pnma quotient counts and the homometric negative control.

Representative exact outputs are in Table S6. Timings and software versions are recorded by the programs. A numerical residual is a convention check, not a substitute for an analytical identity. No measured uncertainty is attached to exact integer counts.

Reference data versus derived data

The input provenance separates four categories: published refined fractional coordinates; published qualitative microscopy/plane descriptions; independently generated ideal structure files; and newly calculated parent occupations, fields, spectra or paths. Parent assignment idealizes the connectivity, not the actual bond geometry. Partial oxygen occupancies belong to average fields. The source articles' diffraction observations are not newly measured data in this work.

For Ca, the coordinate source is explicitly SI Table S1 of ref. 12, including $b = 10.2322$ Å. For the homologous construction, all fields and figures use $f_A(s) = 2f_B(s+2)$ at the stated parent-site origin. The source values, transformations and coordinate conventions are recorded in the reproducibility metadata.

Inheritance of the results

Suppose oxygen and cation relabellings P_O, P_c preserve species and incidence, so $C'P_O = P_cC$. They map binary occupations and the capacity cube one-to-one, preserve the kernel, and carry finite-support variations to finite-support variations. The compatibility, capacity rigidity and domain-restriction statements therefore transfer under this correspondence.

Fourier labels require the corresponding translation action; changing the crystallographic cell changes representation and may fold characters. Enlarging the set of allowed periods instead changes the state space. Transfer of a path extremum also requires an isomorphism of the permitted exchange graph with corresponding endpoints and boundary conditions. Parent-coordinate moments do not automatically become physical moments calculated from displaced atomic positions. This specifies the information that is retained when the same neighbour structure is used in a geometrically distorted material.

Supplementary Note: Experimental minimal rigid topology in $CaMnO_{2.5}$

Experimental inputs

Reller et al. reported three new oxygen-vacancy ordering schemes in $CaMnO_{3-x}$ based on square-pyramidal Mn^{3+} coordination in 1982 [17]. Their 1984 study used selected-area electron diffraction (SAED) and HREM to identify four $CaMnO_{2.5}$ vacancy-order superstructures, including the minimal $(\sqrt{2} \times \sqrt{2})R45°$ mesh (ref. 18, p. 223, Abstract; p. 237, Fig. 18a; p. 239, Table 1). The four observed in-plane meshes are

$$(\sqrt{2} \times n\sqrt{2})R45°, \qquad n = 1, 2, 3, 4, \tag{S55}$$

Section 4(e) describes the $CaMnO_{2.5}$ endpoint as consisting only of MnO_5 square pyramids. The four structures and corresponding [001] electron-diffraction patterns are shown in Fig. 18a–d, with Fig. 18a representing $n = 1$. Their unit-cell dimensions satisfy $a \simeq \sqrt{2}a_c$, $b \simeq n\sqrt{2}a_c$ and $c \simeq a_c$, with $n = 1, 2, 3, 4$ and $c = 3.74$ Å (ref. 18, p. 237). Here a_c is the cubic parent parameter, denoted a_p in our parent-coordinate notation. Independent neutron/X-ray work established five-coordinate, nearly square-pyramidal Mn^{3+} and ordered oxygen vacancies in $CaMnO_{2.5}$ [1].

The $n = 1$ microdomain therefore supplies three topology-level experimental constraints: 1. composition $CaMnO_{2.5}$; 2. parent supercell $(\sqrt{2} \times \sqrt{2})R45° \times a_p$; 3. uniform five-coordinate Mn.

No metric atomic displacement is required for the argument below.

Quotient topology and uniqueness

Choose parent translations

$$a_1 = (1, 1, 0), \qquad a_2 = (1, -1, 0), \qquad a_3 = (0, 0, 1). \tag{S56}$$

The translation sublattice has index

$$|\det[a_1\, a_2\, a_3]| = 2, \tag{S57}$$

so there are two parent B translation classes. They may be labelled by

$$\chi(n) = (-1)^{n_x+n_y}. \tag{S58}$$

$CaMnO_{2.5}$ contains one oxygen vacancy per two parent cells. Consider the orientation of this vacancy.

For a vacancy on a z-oriented parent oxygen edge, the two edge endpoints differ by $e_z = a_3$. They therefore belong to the same B translation class. On the two-class quotient this vacancy contributes missing-oxygen counts

$$(f_B^{(+)}, f_B^{(-)}) = (2, 0) \tag{S59}$$

up to exchange of the two classes. This is incompatible with the experimentally identified all-MnO_5 endpoint, which requires one missing oxygen at every B site.

For a vacancy on an x- or y-oriented edge, the endpoints differ by e_x or e_y, each of which exchanges the two classes because it reverses χ. The missing-oxygen counts are therefore

$$(f_B^{(+)}, f_B^{(-)}) = (1, 1). \tag{S60}$$

The x and y cases are related by parent cubic symmetry. Hence the experimental constraints uniquely determine the parent vacancy topology up to translation and parent-axis permutation.

Choosing the x representative gives

$$x_x(n) = \frac{1 + \chi(n)}{2}, \qquad x_y(n) = x_z(n) = 0. \tag{S61}$$

Direct joint-coordination check

For the B field,

$$\begin{aligned} f_B(n) &= x_x(n) + x_x(n - e_x) \\ &= \frac{1 + \chi(n)}{2} + \frac{1 - \chi(n)}{2} \\ &= 1. \end{aligned} \tag{S62}$$

For an A site, the four incident x-oriented parent oxygen edges have anchors

$$n, \quad n+e_y, \quad n+e_z, \quad n+e_y+e_z. \tag{S63}$$

Because $\chi(n+e_y) = -\chi(n)$ while $\chi(n+e_z) = \chi(n)$,

$$\begin{aligned} f_A(n) &= x_x(n) + x_x(n+e_y) + x_x(n+e_z) + x_x(n+e_y+e_z) \\ &= 2. \end{aligned} \tag{S64}$$

Thus the experimentally identified topology belongs to the uniform

$$BO_5/AO_{10} \tag{S65}$$

joint-coordination fibre.

Singular-only Fourier support

Let

$$c = \frac{1}{6}(1,1,1) \tag{S66}$$

denote the uniform vacancy reference per parent cell. The checkerboard topology contains only a mean term and the character

$$\chi(n) = e^{i(\pi,\pi,0)\cdot n}. \tag{S67}$$

Therefore

$$\operatorname{supp} \widehat{x-c} = \{\Gamma, M_{xy}\}, \qquad M_{xy} = (\pi,\pi,0). \tag{S68}$$

At Γ,

$$\widehat{x-c}(\Gamma) \propto (2,-1,-1), \tag{S69}$$

whose component sum is zero. Since both rows of $C(\Gamma)$ are proportional to $(1,1,1)$, this vector lies in $\ker C(\Gamma)$.

At M_{xy},

$$\widehat{x-c}(M_{xy}) \propto (1,0,0). \tag{S70}$$

Here

$$C(M_{xy}) = \begin{pmatrix} 0 & 0 & 2 \\ 0 & 0 & 0 \end{pmatrix} \tag{S71}$$

in the physical-basis convention, so this vector also belongs to the kernel.

There is no support at a generic rank-2 character. Hence

$$u = 0, \qquad x \in E_L. \tag{S72}$$

Equivalently, the finite-support generator space is orthogonal to this occupancy:

$$G^T x = 0. \tag{S73}$$

Consequence

The capacity-rigidity theorem applies directly:

$$(x + U) \cap [0, 1]^{\mathcal{O}} = \{x\} \tag{S74}$$

for finite-support coordination-preserving variations U on the parent lattice.

The experimental evidence identifies the vacancy-order topology; the local-rewriting rigidity is the mathematical consequence of that topology. No claim about a kinetic barrier, lifetime or thermodynamic stability follows from this statement alone.

Relation to the common Pbam $CaMnO_{2.5}$ structure

The same 1984 study reports four $CaMnO_{2.5}$ vacancy-order superstructures. The widely occurring $n = 2$ structure corresponds to the conventional Pbam topology treated elsewhere in this work and lies in a mixed regular/nonlocal sector. The $n = 1$ microdomain is instead the minimal pure-singular state above.

Thus one experimental chemical system and one stoichiometry realize both an extremal singular topology and a broader mixed topology.

Supplementary Tables

Supplementary Table S1 | Refined Pbam inputs

Fractional positions are those transcribed from Kim et al. SI Table S1 [12] for $Ca_2Mn_2O_5$ and COD 1001352 revision 130149 for the experimental $Sr_2Mn_2O_5$ structure [2]. Special positions are expanded using the Pbam operations in Supplementary Note "Pbam coordinate mappings and registry constructions".

Material	a (Å)	b (Å)	c (Å)
$Ca_2Mn_2O_5$	5.4302	10.2322	3.7443
$Sr_2Mn_2O_5$	5.523	10.761	3.811

Material	A	B	O1
$Ca_2Mn_2O_5$	(0.2990,0.3610,0.5000)	(0.2826,0.1201,0)	(0.2875,0.1027,0.5000)
$Sr_2Mn_2O_5$	(0.2847,0.3631,0.5000)	(0.2583,0.1236,0)	(0.2790,0.0912,0.5000)

Material	O2	O3
$Ca_2Mn_2O_5$	(0.0800,0.2824,0)	(0,0,0)
$Sr_2Mn_2O_5$	(0.5530,0.2259,0)	(0,0,0)

The deterministic assignment uses the central coordinate values above. No independent refinement of these parameters is made.

Supplementary Table S2 | Parent assignment and spectral content

Quantity	$Ca_2Mn_2O_5$	$Sr_2Mn_2O_5$
Parent cells per Pbam unit	4	4
Occupied parent oxygen edges	10	10
Maximum oxygen assignment displacement (Å)	0.546466	0.397425
Minimum nearest-candidate gap (Å)	1.722044	2.057393
f_B at all four B sites	1	1
f_A at all four A sites	2	2
Regular norm squared per Pbam unit	1	1
Singular norm squared per Pbam unit	2/3	2/3

The assignment gap is the distance to the second-closest parent candidate minus the distance to the closest. Norms are for the centred vacancy field, not scattering intensities.

Supplementary Table S3 | Representative Ca reflection classes

Reflection	Parent q (reciprocal-lattice units)	Class	$\Delta F_{\mathrm{vac}}/f_O$	Calculated 2θ, Cu Kα1
(131)	(1.25,-0.25,1)	regular	+2	39.3673°
(061)	(1.5,-1.5,1)	singular M_{xy}	-2	59.5157°
(230)	(1.75,0.25,0)	regular	0	42.5231°

The last column is calculated from the SI lattice, not digitized measured peak positions. The zero contrast in the last row concerns only the two ideal vacancy sites.

Supplementary Table S4 | Nominal homologous parent-site correspondence

Member	Source setting [4]	Parent translation columns	Nominal vacancy-site fractional positions	Parent-model period
n=1	P4/m	(2,1,0),(-1,2,0),(0,0,1), followed by axis interchange	orbit of (1/2,0,0)	5
n=3	P2/m, stated setting	(2,1,0),(1,-3,0),(0,0,1)	(1/2,0,0), (1/2,1/2,0)	7

These nominal-site correspondences support the parent plane model. They are not a claim that every refined atomic displacement or fractional-occupancy correlation has been independently reconstructed. The main construction additionally follows the reported (310) geometry [13].

Supplementary Table S5 | Plane-spacing constructions

Spacing word	Registry cells	Vacancies	B environments	A environments	O/B
4	4	2	4 BO_5	4 AO_{10}	5/2
5	5	2	4 BO_5 + 1 BO_6	4 AO_{10} + 1 AO_{12}	13/5
6	6	2	4 BO_5 + 2 BO_6	4 AO_{10} + 2 AO_{12}	8/3
7	7	2	4 BO_5 + 3 BO_6	4 AO_{10} + 3 AO_{12}	19/7
8	8	2	4 BO_5 + 4 BO_6	4 AO_{10} + 4 AO_{12}	11/4
5,7	12	4	8 BO_5 + 4 BO_6	8 AO_{10} + 4 AO_{12}	8/3

Identical rows of coordination histograms after rescaling do not imply identical site-resolved coordination fields.

Supplementary Table S6 | Exact finite checks

L	rank C	rank G	dim N	Binary construction difference rank (even L)
2	10	3	11	11
3	45	18	18	—
4	108	45	39	39
5	233	108	34	—
6	398	183	67	67

At L=4 the smallest half-area perimeter is eight, with eight equality strips. A path threshold of eight does not connect the two constant masks; a threshold of ten does. One shortest path has perimeter sequence 0,6,8,10,8,10,8,6,0. The general theorem is (S40).

Supplementary References

1. Poeppelmeier, K. R., Leonowicz, M. E., Scanlon, J. C., Longo, J. M. & Yelon, W. B. Structure determination of $CaMnO_3$ and $CaMnO_{2.5}$ by X-ray and neutron methods. *Journal of Solid State Chemistry* **45**, 71–79 (1982). https://doi.org/10.1016/0022-4596(82)90292-4

2. Caignaert, V., Nguyen, N., Hervieu, M. & Raveau, B. $Sr_2Mn_2O_5$, an oxygen-defect perovskite with Mn(III) in square pyramidal coordination. *Materials Research Bulletin* **20**, 479–484 (1985). https://doi.org/10.1016/0025-5408(85)90101-1

3. Caignaert, V., Hervieu, M., Nguyen, N. & Raveau, B. The oxygen defect perovskite $Sr_2Mn_2O_5$: HREM study. *Journal of Solid State Chemistry* **62**, 281–289 (1986). https://doi.org/10.1016/0022-4596(86)90242-2

4. Suescun, L., Chmaissem, O., Mais, J., Dabrowski, B. & Jorgensen, J. D. Crystal structures, charge and oxygen-vacancy ordering in oxygen deficient perovskites SrMnOx (x<2.7). *Journal of Solid State Chemistry* **180**, 1698–1707 (2007). https://doi.org/10.1016/j.jssc.2007.03.020

5. Suescun, L. & Dabrowski, B. $Sr_{4+n}Mn_4^{3+}Mn_n^{4+}O_{10+3n}$: a new homologous series of oxygen-vacancy-ordered perovskites built from $Mn^{3+}O_5$ pyramids and $Mn^{4+}O_6$ octahedra. *Acta Crystallogr B Struct Sci* **64**, 177–186 (2008). https://doi.org/10.1107/s0108768108002760

6. Shin, Y., Poeppelmeier, K. R. & Rondinelli, J. M. Informatics-Based Learning of Oxygen Vacancy Ordering Principles in Oxygen-Deficient Perovskites. *Inorg. Chem.* **63**, 12785–12802 (2024). https://doi.org/10.1021/acs.inorgchem.4c01198

7. Talanov, M. V., Shirokov, V. B. & Talanov, V. M. Anion order in perovskites: a group-theoretical analysis. *Acta Crystallogr A Found Adv* **72**, 222–235 (2016). https://doi.org/10.1107/s2053273315022147

8. Power, S. C. Polynomials for crystal frameworks and the rigid unit mode spectrum. arXiv:1102.2744, version 3 (2013). https://arxiv.org/abs/1102.2744

9. Bergman, D. L., Wu, C. & Balents, L. Band touching from real-space topology in frustrated hopping models. *Phys. Rev. B* **78**, 125104 (2008). https://doi.org/10.1103/physrevb.78.125104

10. Rhim, J. W. & Yang, B. J. Classification of flat bands according to the band-crossing singularity of Bloch wave functions. *Phys. Rev. B* **99**, 045107 (2019). https://doi.org/10.1103/physrevb.99.045107

11. Diaconis, P. & Sturmfels, B. Algebraic algorithms for sampling from conditional distributions. *Ann. Statist.* **26**, 363–397 (1998). https://doi.org/10.1214/aos/1030563990

12. Kim, J., Yin, X., Tsao, K. C., Fang, S. & Yang, H. $Ca_2Mn_2O_5$ as oxygen-deficient perovskite electrocatalyst for oxygen evolution reaction. *J. Am. Chem. Soc.* **136**, 14646–14649 (2014). https://doi.org/10.1021/ja506254g

13. Suescun, L., Hadermann, J. & Dabrowski, B. HR-TEM study of oxygen vacancy ordered $Sr_{4+n}Mn_{4+n}O_{10+3n}$ compounds. *Acta Crystallographica Section A* **70**, C942 (2014). Published microsymposium abstract MS62.O04. https://journals.iucr.org/a/issues/2014/a1/00/a52242/a52242.pdf

14. Molinari, M., Tompsett, D. A., Parker, S. C., Azough, F. & Freer, R. Structural, electronic and thermoelectric behaviour of $CaMnO_3$ and $CaMnO_{3-\delta}$. *J. Mater. Chem. A* **2**, 14109–14117 (2014). https://doi.org/10.1039/c4ta01514b

15. Chiang, C. C. K. & Poeppelmeier, K. R. Structural investigation of oxygen-deficient perovskite $CaMnO_{2.75}$. *Materials Letters* **12**, 102–108 (1991). https://doi.org/10.1016/0167-577x(91)90066-f

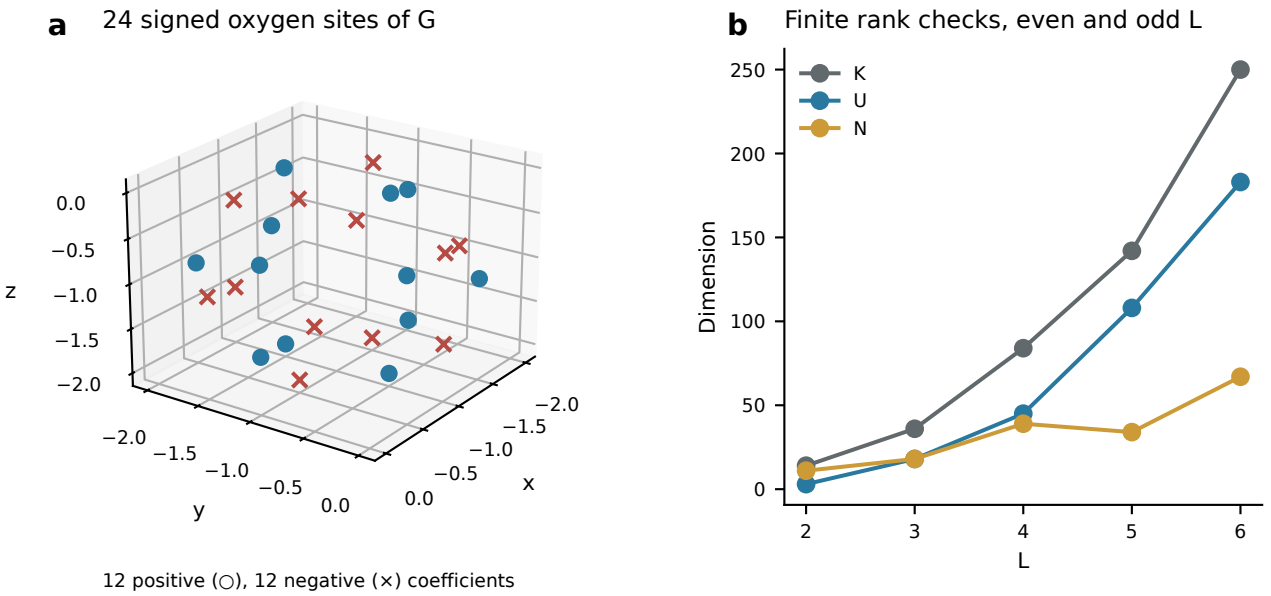
16. Rosenblatt, J. & Seymour, P. D. The Structure of Homometric Sets. *SIAM. J. on Algebraic and Discrete Methods* **3**, 343–350 (1982). https://doi.org/10.1137/0603035

17. Reller, A., Jefferson, D. A., Thomas, J. M., Beyerlein, R. A. & Poeppelmeier, K. R. Three new ordering schemes for oxygen vacancies in $CaMnO_{3-x}$: superlattices based on square-pyramidal co-ordination of Mn^{3+}. *J. Chem. Soc., Chem. Commun.* 1378–1380 (1982). https://doi.org/10.1039/c3982000013 78

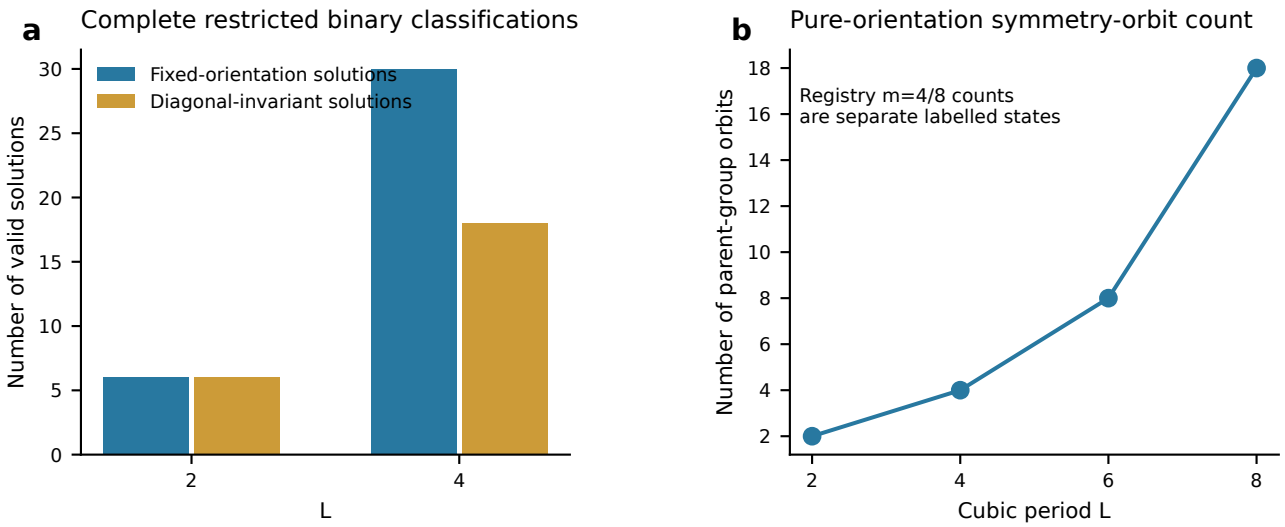
18. Reller, A., Thomas, J. M., Jefferson, D. A. & Uppal, M. K. Superstructures formed by the ordering of vacancies in a selective oxidation catalyst: grossly defective $CaMnO_3$. *Proceedings of the Royal Society of London. A. Mathematical and Physical Sciences* **394**, 223–241 (1984). https://doi.org/10.1098/rspa.1984.0077

19. Nardi, F. R. & Zocca, A. Tunneling behavior of Ising and Potts models in the low-temperature regime. *Stochastic Processes and their Applications* **129**, 4556–4575 (2019). https://doi.org/10.1016/j.spa.2018.12.001

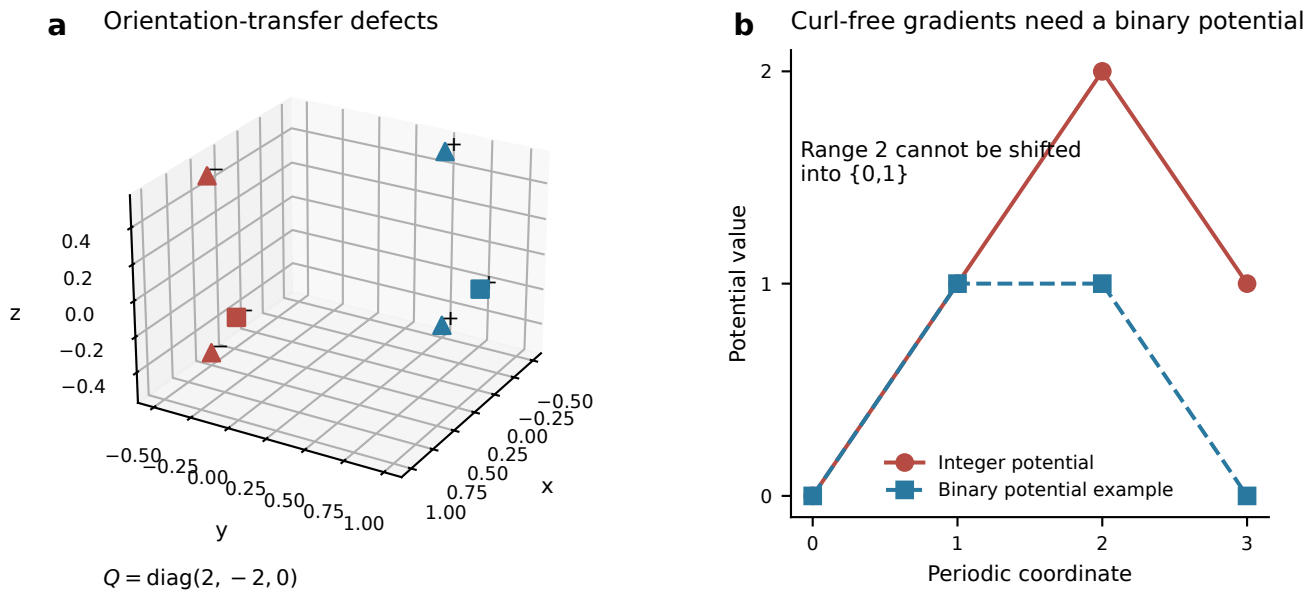
20. Bet, G., Gallo, A. & Nardi, F. R. Critical Configurations and Tube of Typical Trajectories for the Potts and Ising Models with Zero External Field. *J. Stat. Phys.* **184**, 30 (2021). https://doi.org/10.1007/s10955-021-02814-1



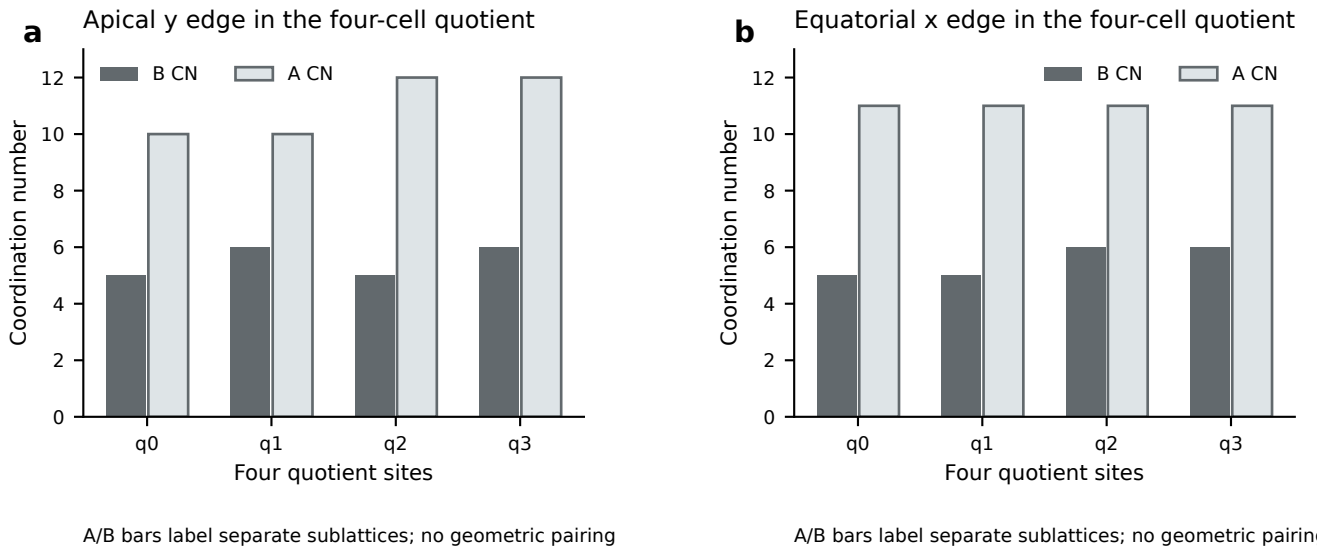
Supplementary Figure S1 | Laurent generator and finite checks. The 24 signed oxygen sites of G, drawn from the expanded monomials with the anchor convention of (S8), have twelve positive and twelve negative coefficients. The positive support is not itself a feasible vacancy subset in every uniform five/ten background. Rank checks for L=2–6 are compared with (S12)–(S13). These checks verify the finite implementation; the primitive-kernel proof is in Supplementary Note "Complete finite-support kernel".



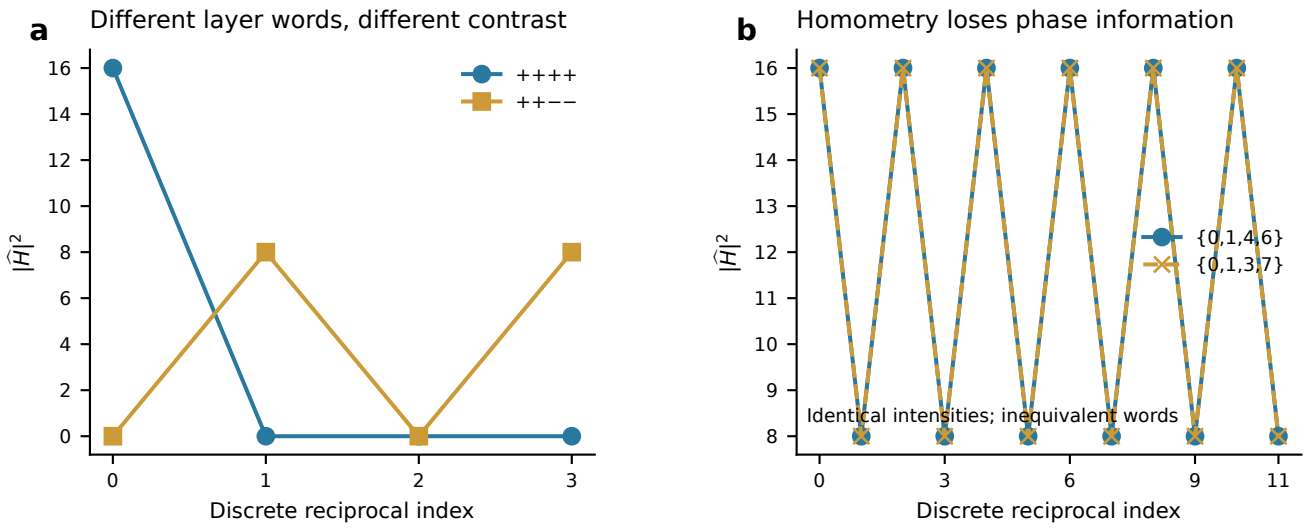
Supplementary Figure S2 | Restricted binary classifications and symmetry counts. The labelled edge and diagonal word counts follow the two necessary-and-sufficient classifications in Supplementary Note "Binary constructions and complete restricted classifications". The pure-orientation symmetry-orbit counts 2,4,8,18 at L=2,4,6,8 agree with (S26). The separate m=4/m=8 registry matching counts refer to labelled stripe states, not these cubic symmetry orbits.



Supplementary Figure S3 | Defect moments and inverse masks. A single orientation transfer gives the signed A/B defects in Supplementary Note "Domain restriction and defect moments" and $Q = \mathrm{diag}(2, -2, 0)$. A valid binary potential is compared with an invalid periodic integer potential; the reconstruction criteria for finite flip masks are proved in Supplementary Note "Complete single-layer channel and exact switching extremum". A periodic integer potential (0,1,2,1) has small curl-free gradients but cannot be translated into a binary mask, illustrating the capacity condition of Supplementary Note "Complete single-layer channel and exact switching extremum".



Supplementary Figure S4 | $CaMnO_{2.75}$ **parent-site classes.** One vacancy in the four-formula-unit Pnma parent gives two BO_5 and two BO_6 sites for either oxygen class. The A fields distinguish the apical parent edge, with two AO_{10} and two AO_{12}, from the equatorial edge, with four AO_{11}. The quotient classes and separate A/B histograms are parent constructions and do not assign the relaxed zig-zag/line structures of ref. 14 or resolve all models of ref. 15.



Supplementary Figure S5 | Layer-word contrast and a homometric pair. $H = (+1, +1, +1, +1)$ and $H = (+1, +1, -1, -1)$ give different ideal superstructure modulation in (S54) despite identical coordination. The plotted layer-word intensity is $|\widehat{H}|^2$; equation (S54) multiplies it by $L^4/4$, a factor of 64 at $L = 4$. Two length-12 words with positive sets {0,1,4,6} and {0,1,3,7} instead have identical cyclic autocorrelation and intensity although they are not related by shift, reversal or complementation. Phase-retaining structural coordinates and intensity-only observations therefore have different reconstruction properties.